

Finite element modeling of reinforced concrete beams externally bonded with PET-FRP laminates

Rami A. Hawileh^{*1}, Maha A. Assad^{1a}, Jamal A. Abdalla^{1b} and M. Z. Naser^{2c}

¹Department of Civil Engineering, American University of Sharjah, Sharjah, United Arab Emirates

²School of Civil and Environmental Engineering & Earth Sciences, Clemson University, 312 Lowry Hall, Clemson, SC 29634

(Received July 15, 2022, Revised September 1, 2022, Accepted September 6, 2023)

Abstract. Fiber-reinforced polymers (FRP) have a proven strength enhancement capability when installed into Reinforced Concrete (RC) beams. The brittle failure of traditional FRP strengthening systems has attracted researchers to develop novel materials with improved strength and ductility properties. One such material is that known as polyethylene terephthalate (PET). This study presents a numerical investigation of the flexural behavior of reinforced concrete beams externally strengthened with PET-FRP systems. This material is distinguished by its large rupture strain, leading to an improvement in the ductility of the strengthened structural members compared to conventional FRPs. A three-dimensional (3-D) finite element (FE) model is developed in this study to predict the load-deflection response of a series of experimentally tested beams published in the literature. The numerical model incorporates constitutive material laws and bond-slip behavior between concrete and the strengthening system. Moreover, the validated model was applied in a parametric study to inspect the effect of concrete compressive strength, PET-FRP sheet length, and reinforcing steel bar diameter on the overall performance of concrete beams externally strengthened with PET-FRP.

Keywords: computational mechanics; concrete structures; externally bonded reinforcement; fiber reinforced plastic (FRP); finite elements method; non-linear analysis; reinforced concrete (RC)

1. Introduction

Strengthening of reinforced concrete (RC) structural members by external bonding to fiber-reinforced polymer (FRP) has been an outstanding and widely accepted retrofitting solution in the structural engineering community. Over the last four decades, several experimental studies were performed on the structural behavior of RC members externally bonded to conventional FRP sheets or plates (Attari *et al.* 2012, Hawileh *et al.* 2014, Naser *et al.* 2019, Salama *et al.* 2019, Abu-Obeidah *et al.* 2019, Zhang *et al.* 2016, Jnaid *et al.* 2013) The most frequent FRPs studied in these investigations are Carbon (CFRP), glass (GFRP), and aramid (AFRP). Findings from such studies converge on the fact that strengthening members using FRP systems greatly enhance the capacity and serviceability of the structural members. The major concerning issue related to the behavior of these members is the brittle failure of FRP sheets in the form of premature debonding (Esmacili *et al.* 2022, Naser *et al.* 2012, Jiao *et*

al. 2017). Given that these materials behave in a linear elastic manner up to rupture at very low strains, the debonding strain at which the FRP sheet is separated from concrete is even lower (i.e., 1-2%).

To overcome the aforementioned drawback of conventional FRPs, and in light of the increased interest in innovative materials, recycling, and sustainable construction, a new type of FRP composite was introduced. This type of FRP is called polyethylene terephthalate (PET) and is manufactured using recycled plastic wastes (Borg *et al.* 2016). In contrast to conventional FRPs, the stress-strain curve of this material is bilinear, and the rupture strain is typically 7% (About 7 times the strain of CFRP) (Mhanna *et al.* 2020). These properties allowed PET-FRP to be a suitable choice for concrete confinement of structural members where ductility is a key consideration, particularly in seismic retrofitting applications. Therefore, several experimental studies were conducted on the behavior of confined concrete with large rupture strain (LRS) (Huang *et al.* 2018, Ispir 2015, Jirawattanasomkul *et al.* 2020, 2021, Ueda *et al.* 2019, Pimanmas *et al.* 2018, Saleem *et al.* 2017, 2018). However, few research papers investigated the flexural response of RC beams strengthened with PET. For example, Liu and Li (2019) conducted an experimental study to investigate the static bearing performance of partially corroded steel in RC beams and columns strengthened with PET-FRP composite. They performed four-point bending tests on beams and found that the ductility and flexural capacity were notably improved for the beams strengthened with PET-FRP. In addition, beams strengthened with PET-FRP experienced an enhanced

*Corresponding author, Professor
E-mail: rhaweeleh@aus.edu

^aGraduate Student
E-mail: g00086297@aus.edu

^bProfessor
E-mail: jabdalla@aus.edu

^cAssistant Professor
E-mail: mznaser@clemson.edu

ductility of 69%.

Another study on the shear strength of RC beams strengthened with PET-FRP was performed by Jirawattanasomkul *et al.* (2014). They strengthened the RC beams in the transverse direction with continuous fully wrapped PET-FRP laminates. They figured out that the shear strength and deformability of the strengthened RC beams were remarkably enhanced. A recent experimental investigation done by Hawileh *et al.* (2022) studied the flexural behavior of RC beams strengthened with PET-FRP laminates. They compared the flexural strength of RC beams strengthened with one and two layers of PET-FRP with a specimen strengthened with one CFRP layer and an unstrengthened beam specimen. When compared to the unstrengthened beam, the specimens strengthened with two PET-FRP layers and one CFRP layer demonstrated an equal and substantial strength enhancement of 47% but with a 33% greater ductility for the PET-FRP strengthened specimen. The specimen strengthened with one PET-FRP layer showed a lower strength enhancement. Despite this, the PET-FRP strengthened beam had a significant ductility that surpassed the unstrengthened beam by 9%. According to the findings of this study, it was revealed that PET-FRP could be a feasible alternative to the traditional FRP strengthening systems.

The flexural performance of strengthened RC beams was studied by various numerical programs where finite element modeling (FE) has been used to simulate the structural response of RC beams strengthened with conventional FRP composites (Assad *et al.* 2022, Choobor *et al.* 2019, Gao *et al.* 2013, Godat *et al.* 2020, Hawileh 2012, Hawileh *et al.* 2011, 2012, 2013, Jirawattanasomkul *et al.* 2018, 2019, Kongwang *et al.* 2019, Kotynia *et al.* 2008, Rasheed *et al.* 2017, Salama *et al.* 2019, Abuodeh *et al.* 2021, Bencardino *et al.* 2014, Haryanto *et al.* 2021, Shrestha *et al.* 2013) These studies were primarily concerned with CFRP strengthened beams. Hawileh *et al.* (2013) investigated the flexural behavior of concrete beams externally strengthened with short-length CFRP plates. They were able to simulate the bond-slip behavior between concrete and the CFRP plate using cohesive 3-D eight-node linear interface elements to capture the debonding process between the CFRP plate and adjacent concrete. In another numerical investigation conducted by Salama *et al.* (2019) to study the flexural behavior of concrete beams strengthened with side-bonded FRP laminates, orthotropic material properties were assigned to 3-D eight-node linear elements to capture the behavior of the FRP laminate in all directions. Kotynia *et al.* (2008) used non-linear and bilinear bond-slip laws to model the bond behavior between FRP and concrete and compared it to the full-bond assumption. Chen *et al.* (2015) used a dynamic analysis approach to represent the debonding failure where it was treated as a dynamic problem to overcome the convergence problems during finite element analysis. Other numerical investigations on different types of FRP include the one conducted by Choobor *et al.* (2019). They have experimentally and numerically tested the flexural performance of strengthened concrete beams with hybrid carbon and basalt FRP sheets. Another study performed by

Kadhim *et al.* (2019) studied the effect of using BFRP in strengthening damaged full-scale RC beams. They included different parameters such as corrosion grade and BFRP wrapping schemes.

Despite the numerous numerical research on strengthening RC beams using conventional FRPs, none of the existing studies considered the behavior of RC beams strengthened with PET-FRP laminates. To bridge this gap in the literature, the purpose of this research is to study the essential parameters that affect the flexural performance of PET-FRP strengthened RC beams through the utilization of a three-dimensional non-linear FE model developed in ANSYS software (2019). The key technical challenge that underscores the necessity of this research is the limited understanding of the flexural behavior of RC beams strengthened with PET-FRP compared to conventional FRPs. As PET-FRP holds promise as an alternative retrofitting solution with improved ductility, investigating its performance is essential to advance retrofitting practices and potentially enhance the safety and resilience of existing structures. The model incorporates the non-linear material properties of concrete cracking and crushing and yielding of steel reinforcement. Moreover, bond-slip action between PET-FRP and concrete was modeled following existing bond-slip laws in the literature. The numerical predictions in terms of load-carrying capacity and load versus mid-span deflection curves are compared and verified with published experimental data (Hawileh *et al.* 2022). The validated model was then expanded to inspect the influence of concrete compressive strength, length of PET-FRP sheet, and rebar diameter on the structural behavior of PET-FRP strengthened RC beams.

2. Description of the FE numerical model

The developed FE model is created to simulate the behavior of experimentally tested RC beams strengthened with CFRP and PET-FRP by Hawileh *et al.* (2022). Full details on tested RC beams are summarized in this section.

2.1 Geometrical configuration

Four 3-D FE models were created using the simulation environment ANSYS 19.2 (ANSYS 2019) The tested RC beams are 1840 mm long with a rectangular section. The width and depth of the specimens are 125 and 240 mm, respectively. The main flexural steel reinforcement is two 10 mm diameter located at a depth of 155 mm from the compression fibers of the beam, and the compression side had reinforcement comprising of two 8 mm diameter. The beam was heavily reinforced with 8 mm diameter steel stirrups at 100 mm spacing along the beam to avoid shear failure. The first specimen which is designated as (B) was left unstrengthened to serve as a control beam, and the second specimen (BC) was strengthened with one layer of CFRP.

On the other hand, the third specimen (BP) was strengthened with one layer of PET-FRP, and the fourth specimen BPP was strengthened with two layers of PET-

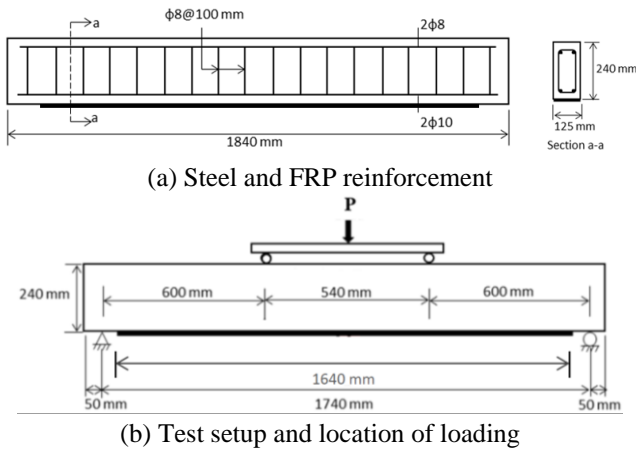


Fig. 1 Tested specimens' details

Table 1 Description of the tested specimens

Beam designation	FRP type	Number of FRP layers
B	-	-
BC	CFRP	1
BP	PET-FRP	1
BPP	PET-FRP	2

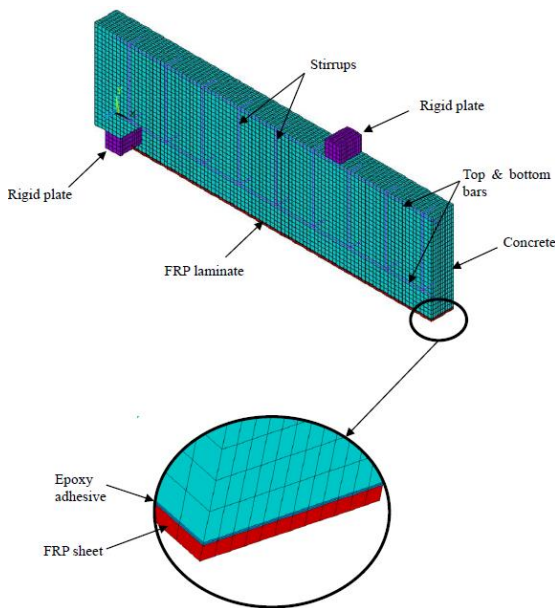


Fig. 2 FE model components

FRP. FRP sheets had a length and width of 1640 mm and 125 mm, respectively. Specimens were tested in flexure by a four-point bending test. Fig. 1 shows an illustrating schematic of the tested RC beams and Table 1 shows the test matrix of the experimental program. It should be noted that a quarter of the beam was built in ANSYS due to symmetry in geometry, loading, boundary conditions, and material properties.

This reduces the number of elements in the FE model and therefore saves considerable computational time. The developed FE model of a quarter of the beam is shown in Figs. 2 and 3.

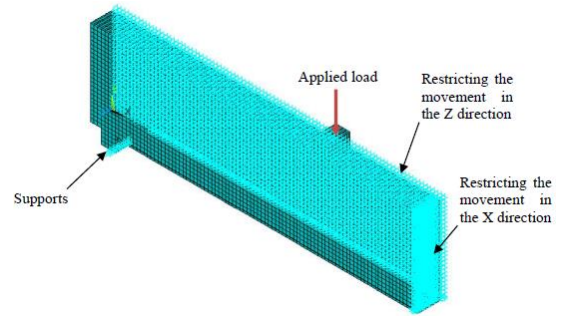


Fig. 3 Symmetry in the X and Z direction

2.2 Elements description

To capture the behavior of each component of the strengthened RC beams, multiple finite element types were utilized using ANSYS 19.2 element library. For instance, concrete was modeled using the SOLID65 element, which is a 3-D eight-node brick element with three translational degrees of freedom at each node. This element can model the behavior of concrete adequately since it has the ability to crack in tension and crush in compression. On the contrary, both main steel reinforcement and stirrups were modeled using the LINK180 3-D truss element defined by two nodes, each with three translational degrees of freedom. It is a uniaxial tension-compression element that is capable of elastic-plastic deformation. Epoxy and FRP layers were modeled using the SOLID185 element. This element is similar to the SOLID65 element but without the nonlinear properties of cracking and crushing. Rigid loading and vertical restraints were also modeled using the SOLID185 element. The bond-slip behavior between FRP sheets and concrete was simulated using INTER205 cohesive elements, 3-D eight-node linear interface element that can capture various interface actions between two surfaces, including debonding. After performing mesh sensitivity analysis, the suitable element size was found to be (10×10×5) mm. The FE model contained a total number of 30300 elements. Movement in the Y direction was restricted at the location of the left support by applying roller supports at the middle nodes. To represent symmetrical conditions, rollers were assigned to the nodes in each plane of symmetry as shown in Fig. 3. The load was applied gradually until failure as a displacement in the Y direction at the top nodes to accurately represent the experimental setup.

2.3 Material properties

The developed FE model is comprised of different materials that were assigned their elastic and inelastic properties, namely, modulus of elasticity, Poisson's ratio, and constitutive laws. According to the experimental tested data, the concrete compressive strength (f'_c), modulus of elasticity, and Poisson's ratio were 36 MPa, 28 GPa, and 0.2, respectively. The nonlinear compressive stress-strain behavior of concrete was simulated using Hognestad *et al.* (1955) model. Following the model's formula, the stress-strain curve of concrete was computed and plotted in Fig. 3.

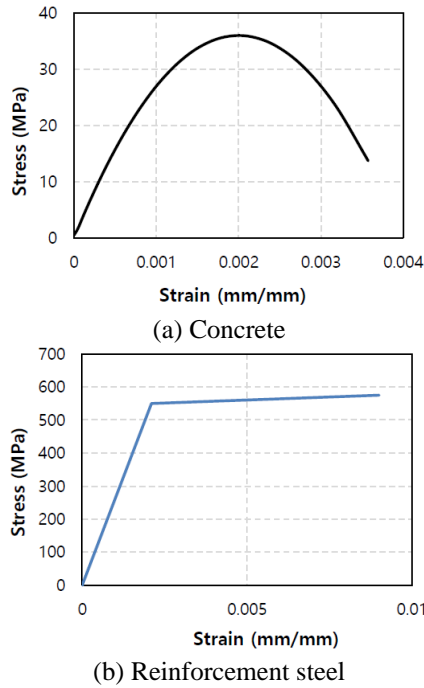


Fig. 4 Stress-strain curve of the constituent materials

In addition, cracking and crushing of concrete were incorporated in the FE model using Willam and Warnke's (1975) concrete model. In this model, the open and closed shear coefficients were assigned as 0.3 and 0.5, respectively. On the other hand, the tensile stress-strain curve is assumed as linear elastic up to the rupture of concrete at a strength of f_t equal to $0.62\sqrt{f'_c}$ and a corresponding strain of ε_t . After that, the concrete exhibits a softening response modeled by a drop in tensile strength to 0.6 f_t . Then, the tensile stress decays linearly to zero at a strain of $6\varepsilon_t$. Regarding the steel reinforcement, the tensile yield strength (f_y) was assigned as 550 MPa. The nonlinear behavior of the steel was modeled as elastic-perfectly plastic as shown in Fig. 4, with a tangent modulus of 200 GPa and Poisson's ratio of 0.3.

The mechanical properties of CFRP and PET-FRP were assigned as per the experimentally tested coupons results (Hawileh *et al.* 2022). The elastic modulus and Poisson's ratio of CFRP were 100 GPa and 0.3, respectively. However, PET-FRP has a bilinear stress-strain relationship with two moduli as shown in Fig. 5. Hence, the first linear elastic modulus is denoted by E_1 , and the second linear elastic modulus is denoted by E_2 . For one layer of PET-FRP, E_1 was 21 GPa and E_2 was 9 GPa. Whereas for two layers of PET-FRP, E_1 and E_2 were 17.3 GPa and 7.2 GPa, respectively. Therefore, PET-FRP material was assigned a bilinear stress-strain relationship in ANSYS where the two moduli were accounted for in the model. Finally, the epoxy adhesive modulus of elasticity was inserted as provided by the manufacturer, and it equals 1 GPa.

2.4 Bond-slip models

To consider the interfacial bond between the FRP layers and concrete surface, bond-slip models were used in the

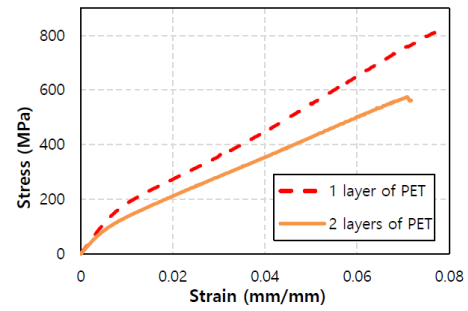


Fig. 5 Stress-strain curve of PET-FRP

Table 2 Bond-slip models parameters

Model	β_w	τ_m (MPa)	s_τ	s_u
Nakaba <i>et al.</i> (2001)	-	6.91	0.0650	0.260
Brosens (2001)	0.82	5.47	0.0381	0.272
Ferracuti <i>et al.</i> (2007)	-	6.91	0.0510	0.204
Lu <i>et al.</i> (2005)	0.71	3.95	0.0513	0.151

developed FE model. As previously mentioned, the debonding phenomenon is simulated using interface element INTER205 and the cohesive zone material model (ANSYS 2019). This model is a function of the slip between the FRP material and concrete. There are many models in the literature that describe the bond-slip relationship between FRP sheets and concrete (Brosens 2001, Dai *et al.* 2005, Ferracuti *et al.* 2007, Jiangtao *et al.* 2017, Lu *et al.* 2005, Nakaba *et al.* 2001). Most of the existing developed bond-slip models in the literature start with an increasing segment up to the ultimate shear stress (τ_m) and its corresponding slip (s_τ). After that, a softening response takes place until the maximum slip (s_u) occurs, which is assumed as four times the value of the ultimate slip ($4s_\tau$). The ultimate shear stress (τ_m), its corresponding slip (s_τ), and the maximum slip (s_u) are inputs in the CZM model in ANSYS. It should be noted that the four bond-slip models were tested in the FE model. Their accuracy to capture the bond-slip behavior was assessed based on the failure modes observed in the experimentally tested beams in Hawileh *et al.* (2022). Table 2 shows the calculated values of τ_m , s_τ , and s_u according to Nakaba *et al.* (2001), Brosens (2001), Ferracuti *et al.* (2007), and Lu *et al.* (2005). Brosens (2001) model was adopted since it showed the most accurate bond-slip behavior of the modeled beams compared to the experimentally tested beams.

Using Brosens K., (2001) model, The value of τ_m and the corresponding slip (s_τ) was calculated using Eqs. (1) and (3)

$$\tau_m = 1.8\beta_w f_t \quad (1)$$

Where τ_m is the maximum bond stress in (MPa).

β_w is the width ratio factor and is calculated as the following

$$\beta_w = \sqrt{\frac{1.5(2 - \frac{b_f}{b_c})}{1 + \frac{b_f}{100}}} \quad (2)$$

Where b_f and b_c is the width of FRP and concrete, respectively.

Table 3 Results and comparison of experimental and FE models

Beam	P_u (FE) (kN)	P_u (Exp.) (kN)	% Difference	δ_u (FE) (mm)	δ_u (Exp.) (mm)	% Difference
B	68.4	65.9	1.21	24.5	23.0	6.5
BC	91.7	97.0	5.46	16.84	18.2	7.5
BP	82.5	81.7	0.98	24.6	24.5	0.4
BPP	100.4	97.1	3.39	25.8	23.8	8.4

f_t is the tensile strength of concrete and it is taken as: $0.62\sqrt{f_c'}$.

The slip at maximum bond stress S_τ is calculated using the following equation

$$S_\tau = 2.5\tau_{max}\left(\frac{t_a}{E_a} + \frac{50}{E_c}\right) \quad (3)$$

Where t_a , E_a and E_c is the thickness of the adhesive layer, modulus of elasticity of the adhesive layer, and modulus of elasticity of concrete, respectively.

Following the above-mentioned formulas, the maximum bond stress (τ_m) and the corresponding slip were calculated to be 4.27 MPa and 0.03, respectively.

2.5 Failure criteria and numerical convergence

Failure is presumed to occur if one or more of the following conditions develop:

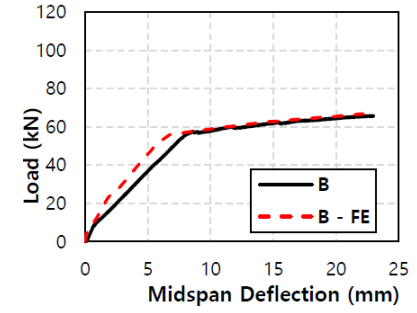
- Yielding of steel reinforcement followed by concrete crushing when the strain in the top compression fibers exceeds 0.003. This is the typical failure mode of the unstrengthened RC beams which was observed in the control specimen.
- Debonding of the FRP sheet from the concrete substrate when the stress in the FRP laminate reaches up to the maximum bond stress (τ_m). This failure mode typically occurs in strengthened RC beams and was initiated in the three strengthened specimens, followed by concrete crushing in the top compression fibers.

Due to the high non-linearity of the constituent materials, large deformations, and the bond-slip action between FRP and concrete, numerical convergence can be hard to achieve. To overcome this convergence hurdle, the force convergence tolerance limit was assigned its maximum value of 0.2. Moreover, the number of load steps was increased around the time step where the solution is struggling to converge.

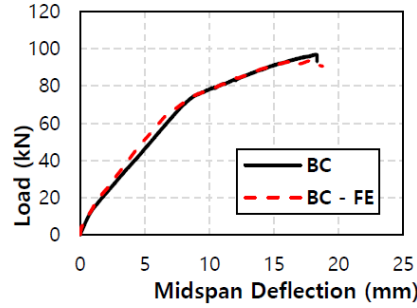
3. Results and discussion

3.1. Validation of the developed FE models

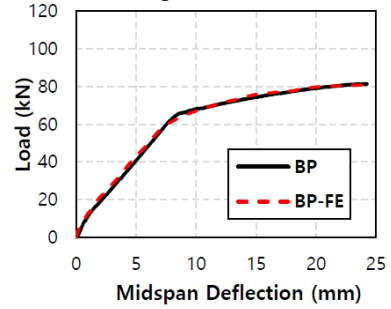
The generated FE model's validity was examined by comparing the FE numerical results with the experimental data reported by Hawileh *et al.* (2022) so that the accuracy of the FE models was assured. Experimental and predicted results were compared for the control specimen (B), the specimen strengthened with one layer of CFRP (BC), and



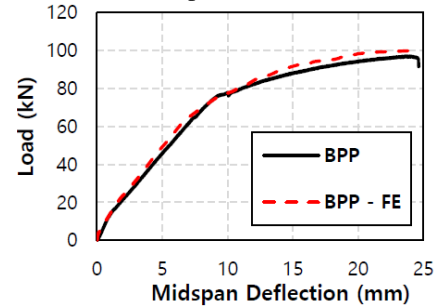
(a) Control specimen (B)



(b) Specimen BC



(c) Specimen BP



(d) Specimen BPP

Fig. 6 Load versus midspan deflection curves of the developed FE models compared to experimental results

the two specimens strengthened with one (PB) and two layers of PET-FRP (PPB). Additionally, a comparison is made for the load-carrying capacity (P_u) and maximum deflection at failure in Table 3 for each specimen. Fig. 6 shows a comparison between the experimental and numerical results for the load versus midspan deflections for each of the four RC beam specimens. A good correlation between the predicted and experimentally tested results are observed for all stages of loading until failure. Also, the difference in the results of the maximum load capacity and maximum deflection was less than 6%. More importantly, the FE simulations predicted the failure modes

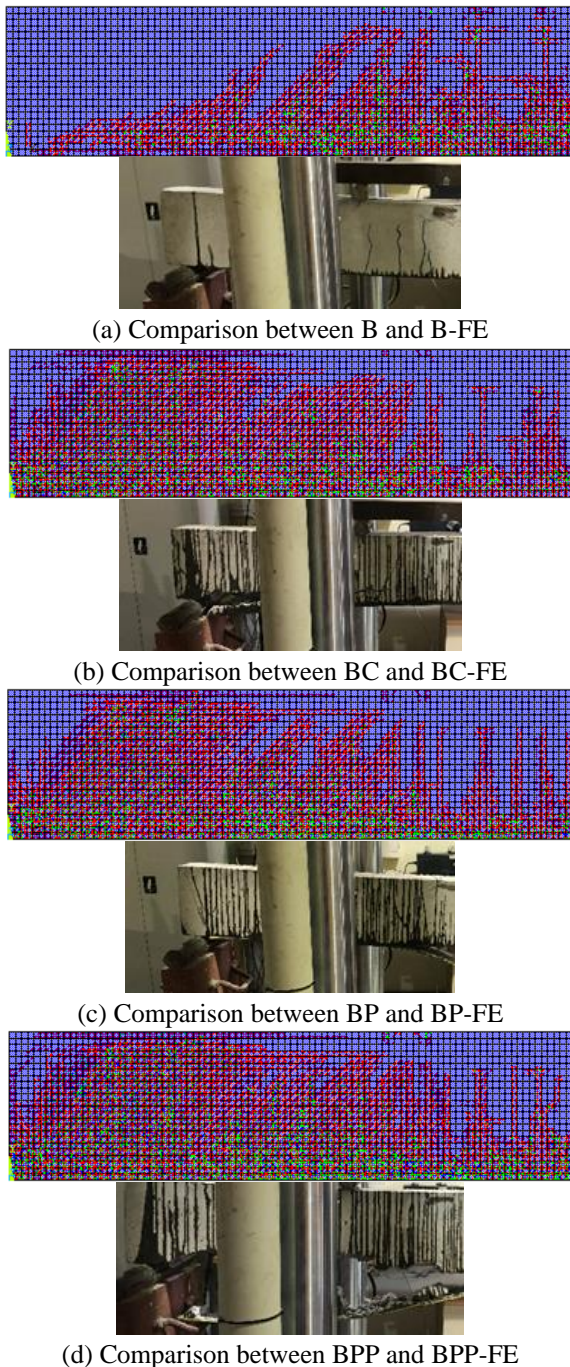


Fig. 2 Cracking patterns of FE models and tested specimens

of the specimens and they agreed with the ones reported in Hawileh *et al.* (2022).

The failure mode reported for the control specimen was the typical crushing of the top fibers after yielding steel reinforcement. Whereas the failure mode observed for the rest of the strengthened specimens was debonding of the FRP sheet from the concrete substrate followed by concrete crushing. However, the specimens strengthened with PET-FRP (BP) and (BPP), showed higher deformation before failure compared to the ones strengthened with CFRP (BC). Cracking patterns were also extracted from the FE models and compared to the experimentally observed patterns presented in Fig. 7. The separation of the FRP sheet as

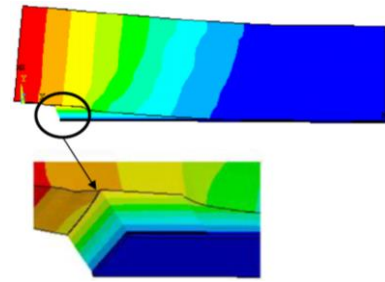


Fig. 8 Typical failure mode of strengthened specimens in the developed FE model

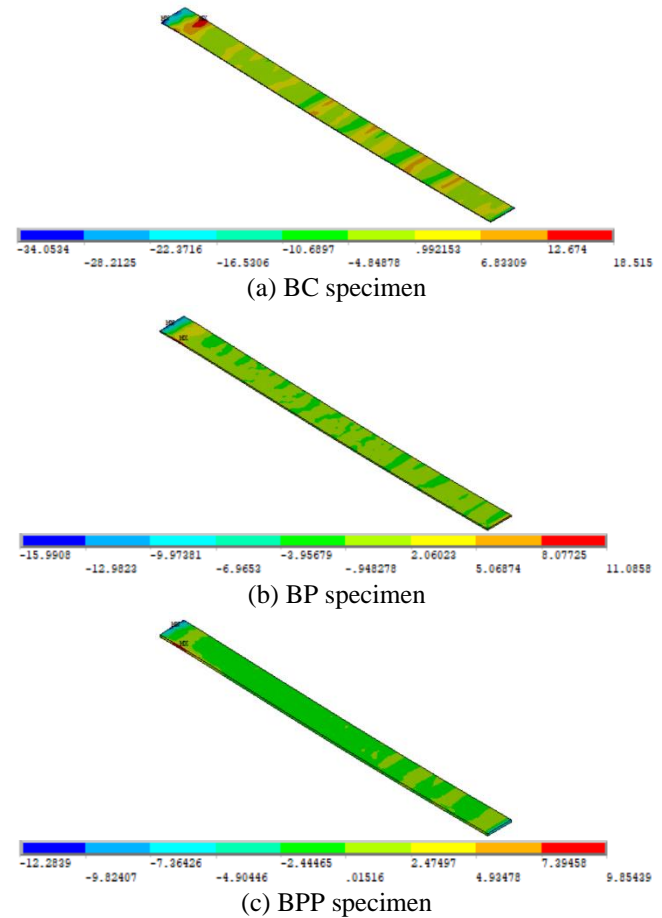


Fig. 9 Shear stress in the FRP sheet

observed for the three strengthened specimens (BC, BP, and BPP) can be seen clearly in Fig. 8. As discussed earlier, this type of failure occurs when the stress in the FRP sheet reaches the maximum bond stress specified by the bond-slip model and assigned in the cohesive zone model (CZM) tool in ANSYS. In Fig. 9, it can be seen that the stress in the FRP sheet has exceeded the maximum bond stress in the three FE models of the strengthened specimens.

4. Parametric study

Using the developed and validated FE model, a parametric study is performed to investigate the flexural behavior of RC beams externally strengthened with PET-

FRP. Therefore, a total of 14 models were simulated, and the BP-FE specimen was taken as a benchmark for this study. The variables tested herein are the concrete compressive strength (f'_c), the reinforcing steel bar diameter, and the length of the PET-FRP sheet.

4.1 Effect of concrete compressive strength (f'_c)

The effect of the concrete compressive strength on the flexural behavior of RC beams was examined by creating six additional FE models, three of them served as unstrengthened control specimens, and the other three were strengthened with PET-FRP. The concrete strength (f'_c) was varied for each model as the following: 45, 50, and 65 MPa. The beams had the same dimensions and reinforcement ratio as the reference model (BP-FE). The control unstrengthened specimens were designated as B-45, B-50, and B-65. Whereas the strengthened specimens were labeled as BP-45, BP-50, and BP-60, referring to f'_c of 45, 50, and 65 MPa, respectively. The previously modeled control and strengthened specimens are denoted by B-36 and BP-36, respectively. The predicted load versus midspan deflection curves for the constructed models are illustrated in Fig. 9. Furthermore, the ultimate attained load and the increase in load capacity were documented in Table 3, in addition to the failure mode of each specimen.

It can be noted that concrete strength has an unremarkable effect on increasing the capacity of unstrengthened RC beams. This can be attributed to the design criteria of these beams in which they are under-reinforced and designed to fail by steel yielding long before concrete crushes. Thus, the yield strength of reinforcing steel determines the capacity of the RC beam. On the contrary, concrete strength had a moderate influence on the strengthened beam performance in terms of load capacity and failure mode. The percentage increase in capacity of beam BP-65 was 59.1% compared to beam BP-36 which depicted a strength gain of 18.1%. This indicates that strengthening RC beams has more influence on beams having higher compressive strength of concrete. It is also observed that the principal failure mode of the strengthened specimens was FRP debonding followed by concrete crushing. One exception for was specimen B-65, which failed only by FRP debonding. This is due to the higher concrete compressive strength which prevented concrete crushing failure.

4.2 Effect of FRP sheet length

In this section, the effect of PET-FRP sheet length on the behavior of RC beams was studied. A total of four models were developed with a varied development length of the FRP sheet beyond the shear span. The results were compared to the full development length model created earlier (termed here as BP-100L) as well as with the value suggested by ACI-440.2R (2017). The first beam was strengthened with a zero-development length of the PET-FRP sheet. This means that the FRP sheet was stopped at the edge of the loading and the percentage of development length from the shear span was equal to zero. This beam

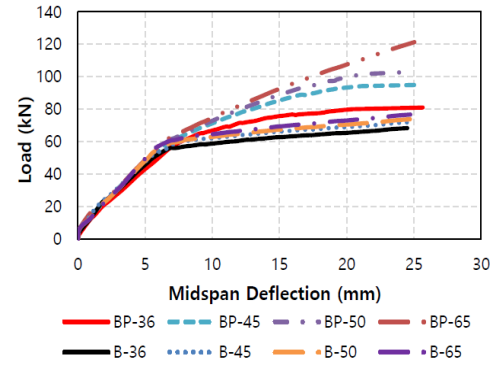


Fig. 10 Effect of varying concrete compressive strength (f'_c)

Table 4 Effect of varying concrete compressive strength (f'_c)

Designation	P_u (kN)	% P_u increase over control specimen	Failure mode
B-36	68.4	-	Steel yielding followed by concrete crushing
B-45	72.1	-	Steel yielding followed by concrete crushing
B-50	73.9	-	Steel yielding followed by concrete crushing
B-60	76.8	-	Steel yielding followed by concrete crushing
BP-36	80.9	18.3	FRP debonding followed by concrete crushing
BP-45	95.1	31.9	FRP debonding followed by concrete crushing
BP-50	103.0	39.4	FRP debonding followed by concrete crushing
BP-65	122.2	59.1	FRP debonding

Table 5 Development length variation

Specimen	Development length (mm)
BP-100L	550
BP-75L	327
BP-50L	218
BP-25L	109
BP-0L	0
ACI 440.2R (2017)	95

was designated as BP-0L. The second beam was strengthened with a 25% development length of the shear span and was labeled as BP-25L. The third and fourth specimens were strengthened with 50% and 75% length of the shear span and were designated as BP-50L and BP-75L, respectively. The value of the recommended development length (l_{df}) by ACI-440.2R (2017) was calculated using Eq. (4).

$$l_{df} = \sqrt{\frac{nE_f t_f}{\sqrt{f'_c}}} \quad (4)$$

Where n is the number of layers, E_f is the modulus of elasticity of the FRP, t_f is the equivalent thickness of the FRP layer.

The load versus midspan displacement behavior of each model was shown in Fig. 10, and the results of the ultimate load, percentage increase in capacity, and failure modes are listed in Table 5. It can be clearly seen from Fig. 10 and Table 4 that the length of the PET-FRP strengthening sheet has a considerable effect on the flexural behavior and the load capacity of the RC beam. The development length of the PET-FRP sheet had a positive influence on the behavior of the RC beam. The higher the length of the PET-FRP sheet, the higher the load capacity of the beam. In fact, decreasing the development length of the sheet below 75% of the shear span had an inverse effect on the flexural capacity of the beam as can be seen in Table 4. It can be observed that the capacity of the beams strengthened with a development length of the sheet that is 50% or lower, examined an even lower peak load than the control specimen. Thus, the development length suggested by ACI-440.2R (2017) is unconservative for PET-FRP laminates and cannot provide the full bond strength between PET-FRP and concrete due to the small modulus of elasticity (E_f) of the PET fibers. Having inadequate FRP length causes the specimens to fail in a brittle manner in the form of FRP debonding which becomes much easier to occur with a lesser development length of the FRP sheet.

4.3 Effect of reinforcing steel bar diameter

The effect of increasing the reinforcing steel bar diameter on the performance of the RC beams is inspected in this section. Four RC beams strengthened with PET-FRP were modeled with different bar diameters, ranging from 12 mm to 18 mm in addition to the validated model which had 10 mm diameter bars. The results of this investigation are presented in Fig. 11 and Table 5, illustrating the load-deflection behavior, load-carrying capacity, and failure mode of each model. It can be observed from Fig. 11 and Table 6 that there is a considerable increase in the ultimate load-carrying capacity in the beams having a 14-mm bar diameter and above. However, these beams experienced a brittle failure in the form of concrete crushing soon after the steel has yielded. This caused the beams to fail at a substantially less deflection than the beams reinforced with 10- and 12-mm bar diameter. The behavior and failure mode of the beam having a bar diameter of 10 and 12 are almost identical. Thus, increasing the bar diameter above 12 mm for the given RC beams negatively affected their behavior in terms of ductility.

5. Conclusions

This study presents the results of a 3-D FE numerical investigation of the flexural behavior of RC beams strengthened with PET-FRP. A total of 18 models were developed to inspect the influence and feasibility of strengthening RC beams with new and sustainable material -Polyethylene Terephthalate (PET-FRP)- in flexure. The developed model accounts for material non-linearities and mechanical interaction between FRP and concrete by incorporating bond-slip models. In the FE model, beams were subjected to a four-point bending test, and their load-

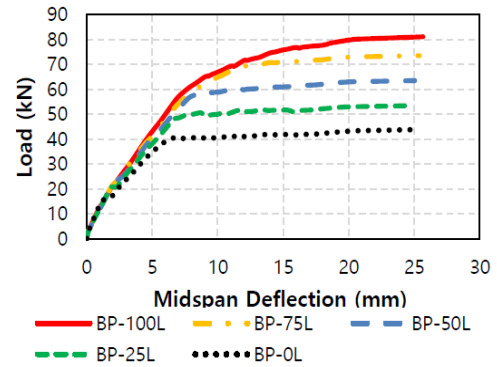


Fig. 11 Effect of varying FRP sheet length

Table 6 Effect of varying FRP sheet length

Designation	P_u (kN)	% P_u increase over control specimen	Failure mode
BP-100L	80.9	18.3	FRP debonding followed by concrete crushing
BP-75L	73.5	7.5	FRP debonding followed by concrete crushing
BP-50L	63.5	-7.2	FRP debonding
BP-25L	53.4	-21.9	FRP debonding
BP-0L	43.7	-36.1	FRP debonding

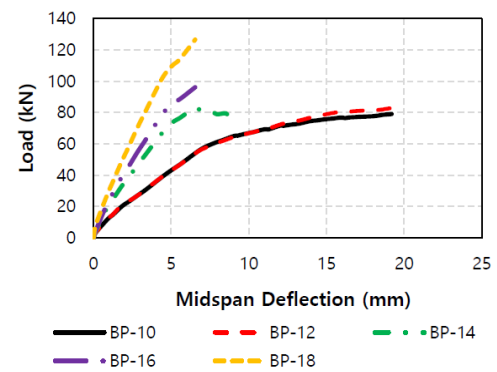


Fig. 12 Effect of varying rebar diameter

Table 7 Effect of varying rebar diameter

Designation	P_u (kN)	% P_u increase over control specimen	Failure mode
BP-10	80.9	18.3	FRP debonding followed by concrete crushing
BP-12	82.9	21.2	FRP debonding followed by concrete crushing
BP-14	83.2	21.6	Steel yielding followed by concrete crushing
BP-16	96.1	40.5	Steel yielding followed by concrete crushing
BP-18	126.5	84.9	Steel yielding followed by concrete crushing

deflection behavior was observed and presented. Four models were validated and compared with published experimental data. Factors affecting the behavior of beams strengthened with PET-FRP were inspected by conducting a parametric study that tested the effect of the concrete compressive strength, the length of the PET-FRP sheet, and the reinforcing steel bar diameter. The following findings

were deducted from this study:

- The developed FE model displayed a good correlation with the experimental data in terms of the load-deflection behavior, ultimate load-carrying capacity, ultimate deflection, and failure mode. The highest recorded deviation of the peak load and ultimate deflection from the experimental data was 5.46 and 8.4%, respectively.
- The development length of the PET-FRP sheet beyond the shear span had a remarkable effect on the capacity and behavior of strengthened RC beams. Precisely, lowering the development length below 75% of the shear span negatively affected the flexural capacity of the beams. This indicated that the development length suggested by the ACI-440.2R equation was inadequate for PET-FRP laminates to develop the desired capacity.
- Increasing the bar diameter of steel reinforcement raised the ultimate load-carrying capacity of the strengthened beams. However, the ductility of these beams was substantially decreased. In addition, the failure mode of the beams reinforced with a bar diameter of 14 and larger, was the brittle concrete crushing right after steel yielding.
- Strengthening RC beams using PET-FRP has more effect on beams with higher compressive strength concrete.

In conclusion, this numerical investigation sheds light on the potential of PET-FRP systems in strengthening RC beams. The developed 3-D finite element model demonstrated great agreement when compared to experimental data. A key finding revealed that lengths below 75% of the shear span adversely impact flexural capacity, underscoring the need for revised guidelines.

6. Future work

Future research related to strengthened RC beams with polyethylene terephthalate (PET) fiber-reinforced polymer (FRP) systems holds substantial promise. The hybridization of this material with other conventional FRP systems (CFRP, GFRP) to create a balance between strength and ductility of strengthened RC beams is an interesting area of research. Mitigating the reduction in ductility observed in RC beams strengthened with conventional FRP sheets could be achieved by using hybrid systems, comprising of both conventional FRPs and PET-FRP. The properties and behavior of such strengthening system should be assessed and studied. Moreover, cost, life cycle assessment, and eco-friendliness evaluations must be explored in the future to assess the environmental impact of PET-FRP as a strengthening material.

Acknowledgment

The support for the research presented in this paper had been provided by Riad T. Al-Sadek Endowed Chair in Civil Engineering at the American University of Sharjah. The support is gratefully appreciated and acknowledged. The

views and conclusions expressed or implied in this study are those of the authors and should not be interpreted as those of the donor or the institution.

References

- Abu-Obeidah, A.S., Abdalla, J.A. and Hawileh, R.A. (2019), "Shear strengthening of deficient concrete beams with marine grade aluminium alloy plates", *Adv. Concrete Constr.*, **7**(4), 249-262. <https://doi.org/10.12989/acc.2019.7.4.249>.
- Akbarzadeh Bengar, H. and Shahmansouri, A.A. (2020), "A new anchorage system for CFRP strips in externally strengthened RC continuous beams", *J. Build. Eng.*, **30**, 101230. <https://doi.org/10.1016/j.jobbe.2020.101230>.
- Al-Obaidi, S., Saeed, Y.M. and Rad, F.N. (2020), "Flexural strengthening of reinforced concrete beams with NSM-CFRP bars using mechanical interlocking", *J. Build. Eng.*, **31**, 101422. <https://doi.org/10.1016/j.jobbe.2020.101422>.
- Al-Saawani, M.A., El-Sayed, A.K. and Al-Negheimish, A.I. (2020), "Effect of shear-span/depth ratio on debonding failures of FRP-strengthened RC beams", *J. Build. Eng.*, **32**, 101771. <https://doi.org/10.1016/j.jobbe.2020.101771>.
- American Concrete Institute and ACI Committee 440 (2017), Guide for the Design and Construction of Externally Bonded FRP Systems for Strengthening Concrete Structures, American Concrete Institute, Farmington Hills, MI, USA.
- ANSYS-Release Version 19.2 (2019), A Finite Element Computer Software and User Manual for Nonlinear Structural Analysis, ANSYS, Inc., Canonsburg, PA, USA.
- Assad, M., Hawileh, R.A. and Abdalla, J.A. (2022), "Modeling the behavior of CFRP-strengthened RC slabs under fire exposure", *Procedia Struct. Integr.*, **42**, 1668-1675. <https://doi.org/10.1016/j.prostr.2022.12.210>.
- Attari, N., Amziane, S. and Chemrouk, M. (2012), "Flexural strengthening of concrete beams using CFRP, GFRP and hybrid FRP sheets", *Constr. Build. Mater.*, **37**, 746-757. <https://doi.org/10.1016/j.conbuildmat.2012.07.052>.
- Bencardino, F. and Condello, A. (2014), "Experimental study and numerical investigation of behavior of RC beams strengthened with steel reinforced grout", *Comput. Concrete*, **14**(6), 711-725. <https://doi.org/10.12989/cac.2014.14.6.711>.
- Borg, R.P., Baldacchino, O. and Ferrara, L. (2016), "Early age performance and mechanical characteristics of recycled PET fibre reinforced concrete", *Constr. Build. Mater.*, **108**, 29-47. <https://doi.org/10.1016/j.conbuildmat.2016.01.029>.
- Brosens, K. (2001), "Anchorage of externally bonded steel plates and CFRP laminates for the strengthening of concrete elements", Doctoral Dissertation, Katholieke Universiteit Leuven, Leuven, Belgium.
- Chen, G.M., Teng, J.G., Chen, J.F. and Xiao, Q.G. (2015), "Finite element modeling of debonding failures in FRP-strengthened RC beams: A dynamic approach", *Comput. Struct.*, **158**, 167-183. <https://doi.org/10.1016/j.compstruc.2015.05.023>.
- Choobbor, S.S., Hawileh, R.A., Abu-Obeidah, A. and Abdalla, J.A. (2019), "Performance of hybrid carbon and basalt FRP sheets in strengthening concrete beams in flexure", *Compos. Struct.*, **227**, 111337. <https://doi.org/10.1016/j.compstruct.2019.111337>.
- Dai, J., Ueda, T. and Sato, Y. (2005), "Development of the nonlinear bond stress-slip model of fiber reinforced plastics sheet-concrete interfaces with a simple method", *J. Compos. Constr.*, **9**(1), 52-62. [https://doi.org/10.1061/\(asce\)1090-0268\(2005\)9:1\(52\)](https://doi.org/10.1061/(asce)1090-0268(2005)9:1(52)).
- Esmaili, J., Aghdam, O.R., Andalibi, K., Kasaei, J. and Gencel, O. (2022), "Experimental and numerical investigations on a novel plate anchorage system to solve FRP debonding problem

- in the strengthened RC beams”, *J. Build. Eng.*, **45**, 103413. <https://doi.org/10.1016/j.jobbe.2021.103413>.
- Ferracuti, B., Savoia, M. and Mazzotti, C. (2007), “Interface law for FRP-concrete delamination”, *Compos. Struct.*, **80**(4), 523-531. <https://doi.org/10.1016/j.compstruct.2006.07.001>.
- Gao, W.Y., Dai, J.G., Teng, J.G. and Chen, G.M. (2013), “Finite element modeling of reinforced concrete beams exposed to fire”, *Eng. Struct.*, **52**, 488-501. <https://doi.org/10.1016/j.engstruct.2013.03.017>.
- Godat, A., Chaallal, O. and Obaidat, Y. (2020), “Non-linear finite-element investigation of the parameters affecting externally-bonded FRP flexural-strengthened RC beams”, *Result. Eng.*, **8**, 100168. <https://doi.org/10.1016/j.rineng.2020.100168>
- Haryanto, Y., Hu, H.T., Han, A.L., Hsiao, F.P., Teng C.J. and Nugroho, L. (2021), “Numerical investigation on RC T-beams strengthened in the negative moment region using NSM FRP rods at various depth of embedment”, *Comput. Concrete*, **28**(4), 347-360. <https://doi.org/10.12989/cac.2021.28.4.347>.
- Hawileh, R.A. (2012), “Nonlinear finite element modeling of RC beams strengthened with NSM FRP rods”, *Constr. Build. Mater.*, **27**(1), 461-471. <https://doi.org/10.1016/j.conbuildmat.2011.07.018>.
- Hawileh, R.A., El-Maaddawy, T.A. and Naser, M.Z. (2012), “Nonlinear finite element modeling of concrete deep beams with openings strengthened with externally-bonded composites”, *Mater. Des.*, **42**, 378-387. <https://doi.org/10.1016/j.matdes.2012.06.004>.
- Hawileh, R.A., Mhanna, H.H., Al Rashed, A., Abdalla, J.A. and Naser, M.Z. (2022), “Flexural behavior of RC beams externally bonded with polyethylene terephthalate (PET) fiber reinforced polymer (FRP) laminates”, *Eng. Struct.*, **256**, 114036. <https://doi.org/10.1016/j.engstruct.2022.114036>.
- Hawileh, R.A., Naser, M.Z. and Abdalla, J.A. (2013), “Finite element simulation of reinforced concrete beams externally strengthened with short-length CFRP plates”, *Compos. Part B: Eng.*, **45**(1), 1722-1730. <https://doi.org/10.1016/j.compositesb.2012.09.032>.
- Hawileh, R.A., Rasheed, H.A., Abdalla, J.A. and Al-Tamimi, A.K. (2014), “Behavior of reinforced concrete beams strengthened with externally bonded hybrid fiber reinforced polymer systems”, *Mater. Des.*, **53**, 972-982. <https://doi.org/10.1016/j.matdes.2013.07.087>.
- Hognestad, E., Hlanson, N.W. and McHenry, D. (1955), “Concrete stress distribution in ultimate strength design”, *J. Proc.*, **52**(12), 455-480. <https://doi.org/10.14359/11609>.
- Huang, L., Zhang, S.S., Yu, T. and Wang, Z.Y. (2018), “Compressive behaviour of large rupture strain FRP-confined concrete-encased steel columns”, *Constr. Build. Mater.*, **183**, 513-522. <https://doi.org/10.1016/j.conbuildmat.2018.06.074>.
- Ispir, M. (2015), “Monotonic and cyclic compression tests on concrete confined with PET-FRP”, *J. Compos. Constr.*, **19**(1), 04014034. [https://doi.org/10.1061/\(asce\)cc.1943-5614.0000490](https://doi.org/10.1061/(asce)cc.1943-5614.0000490).
- Jiangtao, Y., Yichao, W., Kexu, H., Kequan, Y. and Jianzhuang, X. (2017), “The performance of near-surface mounted CFRP strengthened RC beam in fire”, *Fire Saf. J.*, **90**, 86-94. <https://doi.org/10.1016/j.firesaf.2017.04.031>.
- Jiao, P., Soleimani, S., Xu, Q., Cai, L. and Wang, Y. (2017), “Effect of curing conditions on mode-II debonding between FRP and concrete: A prediction model”, *Comput. Concrete*, **20**, 635-643. <https://doi.org/10.12989/cac.2017.20.6.635>.
- Jirawattanasomkul, T., Dai, J.G., Zhang, D., Senda, M. and Ueda, T. (2014), “Experimental study on shear behavior of reinforced-concrete members fully wrapped with large rupture-strain FRP composites”, *J. Compos. Constr.*, **18**(3), 1-12. [https://doi.org/10.1061/\(asce\)cc.1943-5614.0000442](https://doi.org/10.1061/(asce)cc.1943-5614.0000442).
- Jirawattanasomkul, T., Kongwang, N., Jongvivatsakul, P. and Likitlersuang, S. (2018), “Finite element modelling of flexural behaviour of geosynthetic cementitious composite mat (GCCM)”, *Compos. Part B: Eng.*, **154**, 33-42. <https://doi.org/10.1016/j.compositesb.2018.07.052>.
- Jirawattanasomkul, T., Kongwang, N., Jongvivatsakul, P. and Likitlersuang, S. (2019), “Finite element analysis of tensile and puncture behaviours of geosynthetic cementitious composite mat (GCCM)”, *Compos. Part B: Eng.*, **165**, 702-711. <https://doi.org/10.1016/j.compositesb.2019.02.037>.
- Jirawattanasomkul, T., Likitlersuang, S., Wuttiwannasak, N., Ueda, T., Zhang, D. and Shono, M. (2020), “Structural behaviour of pre-damaged reinforced concrete beams strengthened with natural fibre reinforced polymer composites”, *Compos. Struct.*, **244**, 112309. <https://doi.org/10.1016/j.compstruct.2020.112309>.
- Jirawattanasomkul, T., Minakawa, H., Likitlersuang, S., Ueda, T., Dai, J.G., Wuttiwannasak, N. and Kongwang, N. (2021), “Use of water hyacinth waste to produce fibre-reinforced polymer composites for concrete confinement: Mechanical performance and environmental assessment”, *J. Clean. Prod.*, **292**, 126041. <https://doi.org/10.1016/j.jclepro.2021.126041>.
- Jirawattanasomkul, T., Ueda, T., Likitlersuang, S., Zhang, D., Hanwiboonwat, N., Wuttiwannasak, N. and Horsangchai, K. (2019), “Effect of natural fibre reinforced polymers on confined compressive strength of concrete”, *Constr. Build. Mater.*, **223**, 156-164. <https://doi.org/10.1016/j.conbuildmat.2019.06.217>.
- Jnaid, F. and Aboutaha, R. (2013), “Review of design parameters for FRP-RC members detailed according to ACI 440.1R-06”, *Comput. Concrete*, **11**(2), 105-121. <https://doi.org/10.12989/cac.2013.11.2.105>.
- Kadhim, A.M.H., Numan, H.A. and Özakaça, M. (2019), “Flexural strengthening and rehabilitation of reinforced concrete beam using BFRP composites: Finite element approach”, *Adv. Civil Eng.*, **2019**, 1. <https://doi.org/10.1155/2019/4981750>.
- Kotynia, R., Abdel Baky, H., Neale, K.W. and Ebead, U.A. (2008), “Flexural strengthening of RC beams with externally bonded CFRP systems: Test results and 3D nonlinear FE analysis”, **12**(2), 190-201. <https://doi.org/10.1061/ASCE1090-0268200812:2190>.
- Liu, X. and Li, Y. (2019), “Static bearing capacity of partially corrosion-damaged reinforced concrete structures strengthened with PET FRP composites”, *Constr. Build. Mater.*, **211**, 33-43. <https://doi.org/10.1016/j.conbuildmat.2019.03.218>.
- Lu, X.Z., Teng, J.G., Ye, L.P. and Jiang, J.J. (2005), “Bond-slip models for FRP sheets/plates bonded to concrete”, *Eng. Struct.*, **27**(6), 920-937. <https://doi.org/10.1016/j.engstruct.2005.01.014>.
- Mhanna, H.H., Hawileh, R.A., Asce, M., Abuzaid, W., Naser, M.Z., Abdalla, J.A. and Asce, F. (2006), “Experimental investigation and modeling of the thermal effect on the mechanical properties of polyethylene-terephthalate FRP laminates”, *J. Mater. Civil Eng.*, **32**(10), 04020296. [https://doi.org/10.1061/\(ASCE\)MT.1943](https://doi.org/10.1061/(ASCE)MT.1943).
- Nakaba, K., Kanakubo, T., Furuta, T. and Yoshizawa, H. (2001), “Bond behavior between fiber-reinforced polymer laminates and concrete”, *Struct. J.*, **98**(3), 359-367. <https://doi.org/10.14359/10224>.
- Naser, M., Hawileh, R., Abdalla, J.A. and Al-Tamimi, A. (2012), “Bond behavior of CFRP cured laminates: Experimental and numerical investigation”, *J. Eng. Mater. Technol.*, **134**(2), 021002. <https://doi.org/10.1115/1.4003565>.
- Naser, M.Z., Hawileh, R.A. and Abdalla, J.A. (2019), “Fiber-reinforced polymer composites in strengthening reinforced concrete structures: A critical review”, *Eng. Struct.*, **198**, 109542. <https://doi.org/10.1016/j.engstruct.2019.109542>.
- Omar, R. and Abuodeh, R.A.H.J.A.A. (2021), “Finite element modelling of aluminum alloy plated reinforced concrete beams”, *Comput. Concrete*, **27**(6), 585-596. <https://doi.org/10.12989/cac.2021.27.6.585>.

- Pimanmas, A. and Saleem, S. (2018), "Dilation characteristics of PET FRP-confined concrete", *J. Compos. Constr.*, **22**(3), 04018006. [https://doi.org/10.1061/\(ASCE\)CC.1943-5614.0000841](https://doi.org/10.1061/(ASCE)CC.1943-5614.0000841).
- Rasheed, H.A., Abdalla, J., Hawileh, R. and Al-Tamimi, A.K. (2017), "Flexural behavior of reinforced concrete beams strengthened with externally bonded aluminum alloy plates", *Eng. Struct.*, **147**, 473-485. <https://doi.org/10.1016/j.engstruct.2017.05.067>.
- Salama, A.S.D., Hawileh, R.A. and Abdalla, J.A. (2019), "Performance of externally strengthened RC beams with side-bonded CFRP sheets", *Compos. Struct.*, **212**, 281-290. <https://doi.org/10.1016/j.compstruct.2019.01.045>.
- Saleem, S., Hussain, Q. and Pimanmas, A. (2017), "Compressive behavior of PET FRP-confined circular, square, and rectangular Concrete columns", *J. Compos. Constr.*, **21**(3), 04016097. [https://doi.org/10.1061/\(asce\)cc.1943-5614.0000754](https://doi.org/10.1061/(asce)cc.1943-5614.0000754).
- Saleem, S., Pimanmas, A. and Rattanapitikon, W. (2018), "Lateral response of PET FRP-confined concrete", *Constr. Build. Mater.*, **159**, 390-407. <https://doi.org/10.1016/j.conbuildmat.2017.10.116>.
- Shrestha, R., Smith, S.T. and Samali, B. (2013), "Finite element modelling of FRP-strengthened RC beam-column connections with ANSYS", *Comput. Concrete*, **11**(1), 1-20. <https://doi.org/10.12989/cac.2013.11.1.001>.
- Willam, K.J. and Warnke, E.D. (1975), "Constitutive model for the triaxial behavior of concrete", *International Association of Bridge and Structural Engineers, Seminar on Concrete Structure Subjected to Triaxial Stresses*, Bergamo, Italy, May.
- Zhang, D., Wang, Q. and Dong, J. (2016), "Simulation study on CFRP strengthened reinforced concrete beam under four-point bending", *Comput. Concrete*, **17**(3), 407-421. <https://doi.org/10.12989/cac.2016.17.3.407>.